The ATT Strand of AAT·ATT Trinucleotide Repeats Adopts Stable Hairpin Structures Induced by Minor Groove Binding Ligands

Edoardo Trotta,*,‡ Nicoletta Del Grosso,‡ Maura Erba,§ and Maurizio Paci§

Istituto di Medicina Sperimentale, Consiglio Nazionale delle Ricerche, Via del Fosso del Cavaliere 100, 00133 Roma, Italy, and Dipartimento di Scienze e Tecnologie Chimiche, Università di Roma "Tor Vergata", 00133 Roma, Italy

Received January 21, 2000

ABSTRACT: AAT·ATT is the most abundant and also the most frequently polymorphic class of trinucleotide repeats in the human genome. To characterize its structural properties and conformational changes induced by minor groove ligands, $(AAT)_6$ and $(ATT)_6$ oligomers as well as their complexes with DAPI were investigated by electrophoretic mobility and UV thermal stability as well as fluorescence and NMR spectroscopy. The results show that individual $(AAT)_6$ and $(ATT)_6$ strands exist principally as monomeric non-hydrogen-bonded structures. Their individual interaction with DAPI induces the formation of base-paired structures with different thermal stabilities by quite spectroscopically distinct binding mechanisms. In the presence of DAPI, $(ATT)_6$ forms a monomeric hairpin structure stabilized by two ligands located in the minor groove with a strong apparent binding constant of 3.4×10^6 M^{-1}. The DAPI-induced $(ATT)_6$ hairpin is characterized by well-stacked A·T Watson−Crick and T·T wobble base pairs, a high electrophoretic mobility, and a melting temperature of 41 °C. Interaction of DAPI with the complementary $(AAT)_6$ strand favors less stable base-paired structures, and the results are consistent with electrostatic and hydrogen-bond interactions of the ligand with the phosphodiester backbone of $(AAT)_6$ by minor involvement of DNA bases.

Microsatellites are simple tandemly repeated genomic DNA sequences with unknown function. They are highly polymorphic and constitute a major component of the eukaryotic genome (*1*). Over the past few years, particular interest has been focused on CTG·CAG, CGG·CCG, and TTC·GAA trinucleotide repeats since at least 12 human diseases have been found to be associated with their expansion (*2*). The formation of stable unusual intramolecular hairpins appears to be the most probable cause of CTG·CAG and CGG·CCG expansion because of favoring slippage of DNA strands during DNA replication. This hypothesis is strongly supported by experimental evidence that demonstrates the distinctive ability of such DNA sequences in forming intramolecular hairpin structures in vitro (*3*). In addition, DNA loops containing CTG·CAG or CGG·CCG and palindromic sequences are shown to be equally inefficiently repaired in comparison with nonpalindromic sequences, reflecting their ability to form hairpin structures also in vivo (*4*). Triplet repeats can also adopt unusual secondary structures other than a hairpin such as an intramolecular triplex (TCC·GAA) and a tetraplex (CGG, AGG, TGG, and GGG) (*5*, *6*). Such a propensity to adopt unusual secondary structures in addition to the high level of polymorphism, the widespread presence in eukaryotic genome, and the discovered cause of genetic diseases suggest that trinucleotide repeated sequences may play an active role in genetic processes. A deeper understanding of the unusual structural properties of all 10 possible triplet repeats appears to be fundamental for understanding their function in the eukaryotic genome. However, while the structure of GC-rich triplet repeats has been extensively investigated, the structural properties of AT-rich triplet repeats still remain scarcely studied or uncharacterized. In this work, we investigate the structural properties AAT·ATT triplet repeats and their changes induced by the biologically active ligand DAPI.[1]

The AAT·ATT repeat is the most abundant and the most polymorphic triplet repeat in the human genome (*7*). It has not yet been found to extensively expand in vivo as reported for triplet repeats implicated in human diseases. However, expansion of AAT·ATT repeats has been observed during DNA replication in vitro in the presence of double-strand destabilizing factors (*8*) and abasic sites (*9*). Differently from all the other trinucleotide repeats, the AAT·ATT repeat in plasmids shows the unusual propensity to adopt non-hydrogen-bonded structures, suggesting that it may play different roles in gene regulation (*10*).

DAPI (4′,6-diamidino-2-phenylindole) (Figure 1) is a DNA-binding drug largely used as a fluorescent dye for DNA and chromosomes (*11*). It exhibits the property of interfering with the activity of DNA-processing enzymes involved in regulatory and structural functions such as DNA polymerase I (*12*), RNA polymerases (*12*−*14*), topoisomerases (*12*, *15*−*17*), DNA ligase (*12*), exonuclease III (*12*), DNAase I (*18*),

* Corresponding author. Fax: +39-0649934257. E-mail: Edoardo.Trotta@ims.rm.cnr.it.

‡ Consiglio Nazionale delle Ricerche.

§ Università di Roma "Tor Vergata".

[1] Abbreviations: DAPI, 4′,6-diamidino-2-phenylindole; NMR, nuclear magnetic resonance; NOE, nuclear Overhauser effect; NOESY, NOE spectroscopy; TOCSY, total correlated spectroscopy; TPPI, time-proportional phase incrementation.

10.1021/bi0001473 CCC: $19.00 © 2000 American Chemical Society
Published on Web 05/18/2000

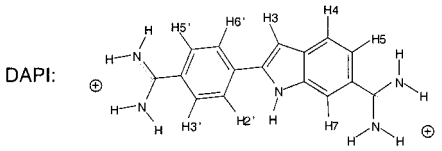

(ATT)6: 5'-ATTATTATTATTATTATT-3'

(AAT)6: 5'-AATAATAATAATAATAAT-3'

(AT)9: 5'-ATATATATATATATATAT-3'

(AT)5: 5'-ATATATATAT-3'

FIGURE 1: Chemical structure and numbering system for DAPI and nucleotide sequences of $(ATT)_6$, $(AAT)_6$, $(AT)_9$, and $(AT)_5$ DNA oligomers.

and restriction endonucleases (*18*). Due to its biological activity and sequence-dependent binding properties, its complexes with natural and synthetic DNA have been the object of intense investigation. DAPI preferentially binds DNA into the minor groove of two or more consecutive A·T base pairs (*19*) or T·T mismatches flanked by A·T base pairs (*20*), whereas it exhibits a quite different binding geometry and a lower affinity with DNA sequences containing no adjacent A·T base pairs (*21*−*25*). A single and exclusive binding mechanism of DAPI in the minor groove of AT sequences has been reported and characterized by X-ray and NMR spectroscopy (*19*, *20*, *26*−*28*). In contrast, experimental evidence for binding mechanisms different from minor groove interaction has been reported for G·C or nonconsecutive A·T base pairs: intercalation (*21*−*23*, *29*), major groove binding (*25*), and $\pi-\pi$ stacking interactions with double-helix ends (*28*).

In this work, we provide evidence that a classical minor groove ligand induces stable hairpin structures on the ATT strand of AAT·ATT trinucleotide repeats. This demonstrates a new structural effect of AT specific minor groove ligands on a large class of microsatellite DNA. Also, this result reveals the propensity of AAT·ATT repeats to form hairpins modulated by DNA ligands, suggesting a model for the possible regulation mechanism associated with the formation of secondary structures in vivo.

EXPERIMENTAL PROCEDURES

Materials. The DNA oligomers $(ATT)_6$, $(AAT)_6$, $(AT)_9$, and $(AT)_5$ (Figure 1) were synthesized by an Applied Biosystems 391 instrument. After deprotection, the oligomers in a 0.5 M NaCl solution were purified by at least four precipitations with 2 volumes of ethanol at −20 °C and finally desalted by chromatography on Sephadex G-10. DNA oligomer concentrations were determined spectrophotometrically by using the extinction coefficients calculated as previously reported (*30*) and their purities checked by ^{1}H NMR spectroscopy and denaturing polyacrylamide gel electrophoresis. DAPI and Hoechst 33258 were purchased from Sigma, their purities checked by ^{1}H NMR, and their concentrations measured spectrophotometrically using an ϵ_{340} of 27 000 M^{-1} cm^{-1} (*11*) and an ϵ_{338} of 42 000 M^{-1} cm^{-1} (*31*), respectively. All DNA samples were incubated for 5 min at 80 °C and slowly cooled at room temperature before spectroscopic and electrophoretic analyses were carried out.

NMR Spectroscopy. NMR spectra were obtained using a Bruker AM 400 instrument operating at 400 MHz. D_2O and H_2O one-dimensional NMR spectra were run over spectral widths of about 10 and 20 ppm, respectively, and accumulated on 16K or 32K of memory with the carrier frequency centered on the water resonance.

Two-dimensional NMR spectra were typically run in the phase-sensitive mode using TPPI (*32*), with a recycle delay of 2.2 s, recording from 400 to 600 experiments over 2K of memory. Correlation spectra were recorded by using TOCSY experiments with a MLEV-17 pulse sequence to substitute the spin-lock period (*33*, *34*). Two-dimensional exchange spectroscopy was performed using NOESY experiments (*35*) at mixing times of 70 and 250 ms. Suppression of the water signal in one- and two-dimensional spectra of H_2O samples was achieved with a 1−1 spin-echo pulse sequence ($90_x-t-90_{-x}-D-90_\phi-2t-90_{-\phi}-D-$AQ) (*36*), using a D of 50 μs, a t of 85 μs, and a carrier frequency adjusted to the water resonance. All data were processed on a Silicon Graphics workstation using the program NMRpipe (*37*).

NMR samples were 100 mM NaCl and buffered with 10 mM sodium phosphate at pH 7.00. Titration experiments were performed by adding small concentrated volumes of a drug solution to the DNA samples. To check the stability of the interaction, at least two spectra at different times were acquired for every drug:duplex molar ratio.

Electrophoresis. Electrophoretic conformational analysis was performed at 4 and 25 °C in a nondenaturing polyacrylamide gel (15%, 29:1 monomer:bis ratio, 20 cm × 20 cm × 0.08 cm) buffered in TBE (90 mM Tris-borate and 2 mM EDTA at pH 8.3). The loading DNA samples were 0.05−0.125 ODU at 260 nm in 10 μL of 100 mM NaCl. Glycerol (5% v/v) was added to the samples just before the run. A base pairs:DAPI molar ratio of 3 was used for the drug−DNA samples. Nondenaturing polyacrylamide gels were analyzed under UV light to detect DAPI−DNA fluorescent complexes and successively stained with silver to also detect nonfluorescent complexes and DAPI-free DNA oligomers.

Denaturing polyacrylamide gel electrophoresis (15%, 39:1 monomer:bis ratio, 7 M urea) was performed at 25 °C in TBE. Samples were suspended in 5 μL of H_2O and loaded with an equal volume of loading buffer (98% formamide, 10 mM EDTA, 0.025% xylene cyanol, and 0.025% bromophenol blue) after heat denaturation for 5 min at 90 °C. Denaturing polyacrylamide gels were stained with silver.

Fluorescence Spectroscopy. Fluorescence spectra were recorded on a SPEX FluoroMax photon counting spectrofluorometer equipped with a thermostated cell holder. Excitation (350 nm) and emission (448 nm) with a 1.5 nm bandpass were used, and spectra were corrected for the background signal. The absorbance at the excitation wavelength was less than 0.027 ([DAPI] = 0.96 μM), making the inner filter effects negligible. The experiments were performed at 15 °C, in 10 mM Tris (pH 7.2) and 100 mM NaCl, by adding an increasing amount of DNA oligomers to DAPI solutions. Constancy of the DAPI concentration was achieved by adding a DNA solution containing DAPI with the same molarity as the initial DNA-free solution.

UV Melting Experiments. UV thermal melting studies were performed on a Hewlett-Packard diode array spectrophotometer (model 8452A) equipped with a thermostated cuvette holder. The samples were heated from 2 to 66−80 °C in increments of 1 °C followed by equilibration for 5 min. Absorbance spectra were taken every 1 °C after the equilibration period. To avoid evaporation of the solvent, a

5 mm layer of liquid paraffin was placed on the surface of the samples and the cuvette was tightly stopped with a Teflon plug and Parafilm. The cuvette-holding chamber was dried by flushing it with N_2 gas to avoid condensation of water vapor at low temperatures. Each sample was 0.7−1 OD_{260}/mL in 10 mM Tris-HCl (pH 7.5) and 100 mM NaCl with a base pair:drug molar ratio of 3 for the DAPI−DNA samples. Hyperchromicity (percent) at the temperature T °C was given by $\{[A_{(T\ °C)} - A_{(2\ °C)}]/A_{(2\ °C)}\} \times 100$, where $A_{(T\ °C)}$ and $A_{(2\ °C)}$ represent the absorption (260 nm) at T °C and 2 °C, respectively. The melting temperatures (T_m) were estimated from the maximum of the first-derivative curve of the absorbance at 260 nm versus temperature.

Calculation of Binding Constants. Binding constants were calculated from fluorescence titration experiments by using the formula of Kelly et al. for nearly stoichiometric (tight-binding) titration, $K_{app} = Ø/[(1 - Ø)^2[P_0]]$ (*38*), where K_{app} is the apparent binding constant, Ø is the fraction of DAPI saturation measured at the stoichiometric DNA site concentration, and $[P_0]$ is the total concentration of DAPI. For the moderately tight interaction of DAPI with $(ATT)_6$, the binding constant was also estimated by fitting the data with a theoretical curve generated by the mathematical model developed by Epstein et al. (*39*) which accounts for cooperative and noncooperative binding of ligands to a finite one-dimensional lattice.

Molecular Modeling. Molecular modeling and calculations were carried out using INSIGHTII version 2.3.0 and DISCOVER version 2.9.5 software packages (Molecular Simulations). The AMBER force field was employed in all calculations, and partial atomic charges for DAPI were used as previously reported (*40*). Calculations were performed in vacuo with a distance-dependent dielectric constant (ϵ) to simulate solvent effects in molecular mechanics ($\epsilon = 4r_{ij}$) and dynamics ($\epsilon = r_{ij}$) calculations. A cutoff of 18 Å with a switching distance of 2 Å was used for nonbonded interactions, and 1,4 electrostatic interactions were scaled by 0.5. Counterions were simulated by reducing to −0.2 the net charge of phosphate groups. NMR results providing the presence of base pair hydrogen bonds and the anti conformation of glycosidic torsion angles were considered in all calculations by incorporating distance restraints to reinforce the hydrogen bonds of the five Watson−Crick A·T base pairs of the hairpin stem and glycosidic torsion angle restraints of the 14 stem nucleotides. Hydrogen bond restraints (a lower bound of 2.72 Å and an upper bound of 3.2 Å for A N6−T O4 and A N1−T N3 distances) and glycosidic dihedral angle restraints (a lower bound of −200° and an upper bound of −85° for adenine O4′−C1′−N9−C4 and thymine O4′−C1′−N1−C2 angles) were applied with force constants of 50 kcal mol^{-1} $Å^{-2}$ and 50 kcal mol^{-1} rad^{-2}, respectively.

The initial $(ATT)_6$ hairpin was built assuming a loop of four bases and a base-paired stem in a B-type conformation. The initial DNA structure was subjected to one cycle of energy minimization followed by 100 ps of 300 K constant-temperature molecular dynamics. The average structure of the last 5 ps was energy-minimized and used to build initial DAPI−hairpin complexes for calculations. Two DAPI molecules per hairpin were placed into the minor groove by superimposing the DNA binding site and DAPI with our previously characterized DAPI−DNA minor groove complexes (*19*, *20*, *28*). A binding site size of four base pairs, nine base pairs per hairpin (loop base pairs were included), and the two possible orientations of DAPI in the minor groove of each site were considered, leading to a combination of 12 starting structures of the complex. The resulting structures were energy minimized and then subjected at 10 ps of 200 K constant-temperature molecular dynamics simulation followed by a gradual increase of simulation temperature to 300 K (10 ps) and 90 ps of 300 K constant-temperature simulation. The average structures of the last 2 ps were energy minimized until the maximum derivative was less than 0.5 kcal/Å and then subjected to 500 cycles of unrestrained energy minimization. At last, the trajectory of molecular dynamics simulations and energy contributions of the final 12 structures of the complex were analyzed and compared by using the Analysis module of the INSIGHTII program.

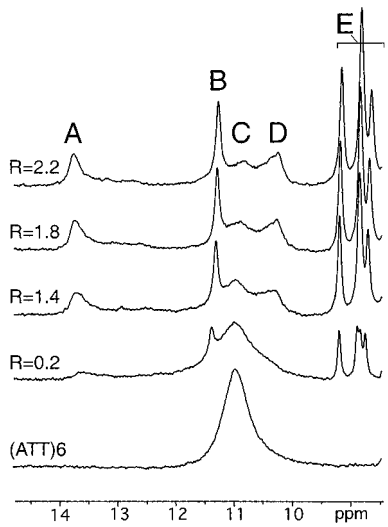

FIGURE 2: Imino proton spectra of $(ATT)_6$− and $(ATT)_6$−DAPI complexes. Spectra were acquired at 298 K with a 1−1 spin-echo pulse sequence to suppress the water signal. *R* is the DAPI:$(ATT)_6$ molar ratio in the complexes. The letters indicate the resonance assigned to the H3 imino protons of Watson−Crick A·T base pairs (A), the NH indole proton of DAPI (B), the H3 imino protons of unpaired thymine (C), the H3 imino protons of T·T mismatched base pairs (D), and the DAPI amino protons (E).

RESULTS

NMR of $(ATT)_6$. Figure 2 reports the imino proton spectra acquired at 298 K of $(ATT)_6$ and DAPI−$(ATT)_6$ complexes at different drug:oligomer molar ratios. In the absence of DAPI, the imino region of the DNA spectrum is characterized by the presence of a single broad peak at about 11 ppm, consistent with non-hydrogen-bonded thymine imino protons previously reported for d(TTTT) (11.2 ppm) (*41*) and quite shifted from those expected for Watson−Crick A·T base pairs (13−14.5 ppm) (*42*). The addition of DAPI to the DNA solution causes a decrease in the intensity of this peak and the appearance of new growing peaks at about 14, 11.4, and 10.3 ppm which provide evidence of formation of a DAPI−DNA complex slowly exchanging on the NMR time scale with free species. Chemical shifts of these new resonances are consistent with those previously reported for the minor groove complex of DAPI with the ATT site of $[d(GCGATTCGC)]_2$ and attributed to the A·T Watson−Crick hydrogen-bonded NH (peak A in Figure 2), DAPI indole NH (peak B in Figure 2), and T·T mismatch hydrogen-bonded NH (peak

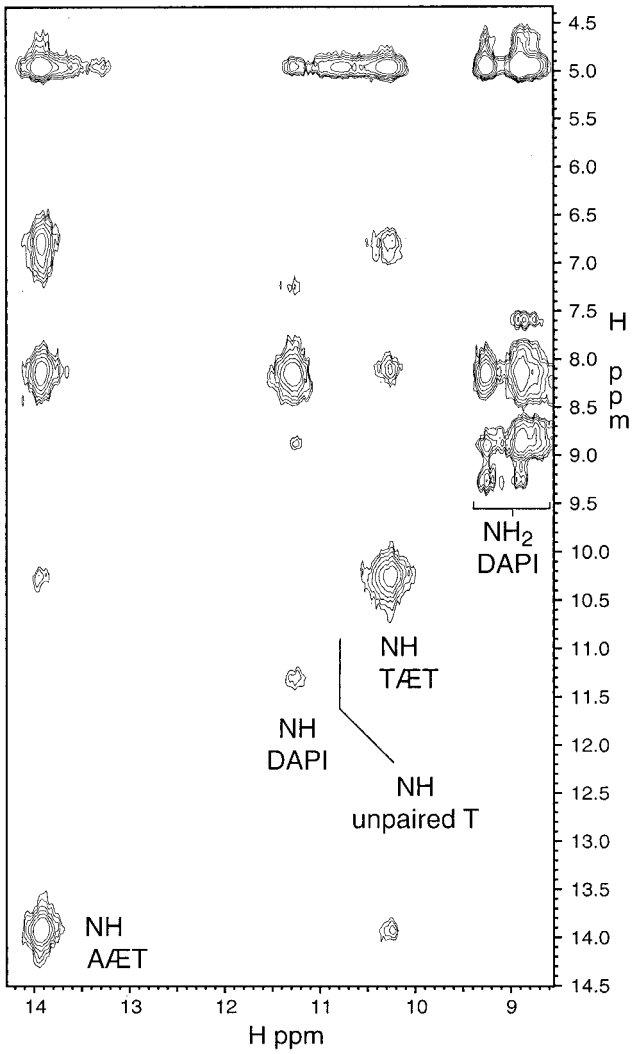

FIGURE 3: Expanded region of a NOESY spectrum of a 2.2:1 DAPI−$(ATT)_6$ complex. The spectrum was acquired at 12 °C, with a mixing time of 250 ms, in 90% H_2O/10% D_2O buffer.

D in Figure 2) (*20*). This assignment is also supported by the observation of a NOE correlation between imino resonances of the adjacent thymines belonging to A·T and T·T base pairs (Figure 3). In addition, both resonances exhibit NOEs with an exchangeable proton resonance at 6.8 ppm, which can be safely attributed to the NH_2 of adenine for its chemical shift value and exchanging property, and with resonances in the region expected for adenine H2 protons (about 8.1 ppm). Also, resonances of imino protons belonging to unpaired thymines exhibit a chemical exchange cross-peak with the water signal (4.9 ppm) but do not exhibit diagonal peaks, providing evidence of their expected fast exchange rate with water protons (Figure 3). The resonances of the complex around 9 ppm (peaks E in Figure 2) belong to amino protons of DAPI as evaluated by intramolecular NOEs (Figure 3) and their chemical shift values (*29*). Broad and weak resonances due to exchangeable protons other than those described above are also observed around 13 ppm (Figure 2). Because of their chemical shift values, the reduced intensity, and the greater accessibility to water protons compared to those of the other exchangeable protons, these resonances could be attributed to imino protons of terminal A·T base pairs or, in the case of the hairpin structure, to stem A·T base pairs next to the loop. Spectral changes of DNA resonances in H_2O titration experiments were observed up to a DAPI:$(ATT)_6$ molar ratio (R) of about 2. For an R of more than 2, the intensity of DNA peaks did not change as DAPI was further added. In particular, the DNA resonance assigned to the NH of unpaired thymines (peak C in Figure 2) is still present when $R = 2$ and its intensity does not change furthermore for higher R values. This result provides evidence of a binding stoichiometry of two DAPI molecules per $(ATT)_6$ and suggests the presence of single-stranded regions, such as unpaired loops or slipped ends, in the final structure of the complex. The observation of imino and amino proton resonances of DAPI at high temperatures, which were not observed in DNA-free DAPI solutions, suggests their involvement in hydrogen bonds with DNA, consistent with the NMR results of minor groove complexes reported in the literature (*19*, *20*, *28*).

The repetitive nature of $(ATT)_6$ and the slow to intermediate exchange rate between free and bound species caused overlapping and line broadening of nonexchangeable DNA resonances in ^1H NMR spectra of $(ATT)_6$−DAPI samples. For this reason, spectra acquired in D_2O appeared to be not easily interpreted to allow a complete sequential assignment and to obtain experimental distances and dihedral bond angles for the molecular modeling of the complex. However, from the combined analysis of titration experiments and dipolar as well as scalar two-dimensional spectra, we were able to assign drug resonances and to distinguish DNA resonances belonging to adenine and thymine residues as well as to different groups such as H1′, H2′/H2″, H3′, H6, H8/H2, H4′/H5′/H5″, and CH_3. This was sufficient to characterize the geometry of binding of DAPI to $(ATT)_6$.

The addition of DAPI to an $(ATT)_6$ solution causes a sensible line broadening of all DNA signals and the appearance of high-field resonances in all the regions of the D_2O spectrum. In particular, strong upfield shifts induced by DAPI were observed for H1′ and H4′/H5′/H5″ DNA protons. Moreover, consistent with NMR titration in H_2O, significant changes in the DNA spectrum in D_2O occur up to a DAPI:$(ATT)_6$ molar ratio of 2. In contrast, DAPI resonances, assigned as previously reported (*19*, *29*), appear to be weakly shifted upon binding. Figure 4B shows a region of a NOESY spectrum of the complex acquired in D_2O (Figure 4A) where intermolecular NOEs are indicated. As shown, DAPI phenyl protons (H2′/H3′/H5′/H6′) exhibit intermolecular NOEs with H4′/H5′/H5″ (peaks a in Figure 4B) and H1′ (peaks b in Figure 4B) DNA protons, while drug indole protons (H3, H4, and H5) exhibit NOEs only with H4′/H5′/H5″ DNA protons (peaks c−e in Figure 4B). This is consistent with intermolecular NOEs previously reported for DAPI minor groove complexes (*19*, *20*, *28*).

Finally, NOESY spectra of the DAPI−$(ATT)_6$ complex exhibit weak or no H1′−H6/H8 and H2″−H4′ intranucleotide NOEs.

NMR Data of $(AAT)_6$. Figure 5 shows the imino proton spectra of $(AAT)_6$ and the 2:1 DAPI−$(AAT)_6$ complex acquired at different temperatures. DAPI-free $(AAT)_6$ exhibits a broad resonance at about 11 ppm that is typical of non-hydrogen-bonded imino protons and, at 8 °C, a weak resonance (13 ppm) in the range expected for hydrogen-bonded Watson−Crick A·T base pairs. The addition of DAPI to $(AAT)_6$ increases the intensity and the thermal stability of this last resonance but slightly changes its chemical shift.

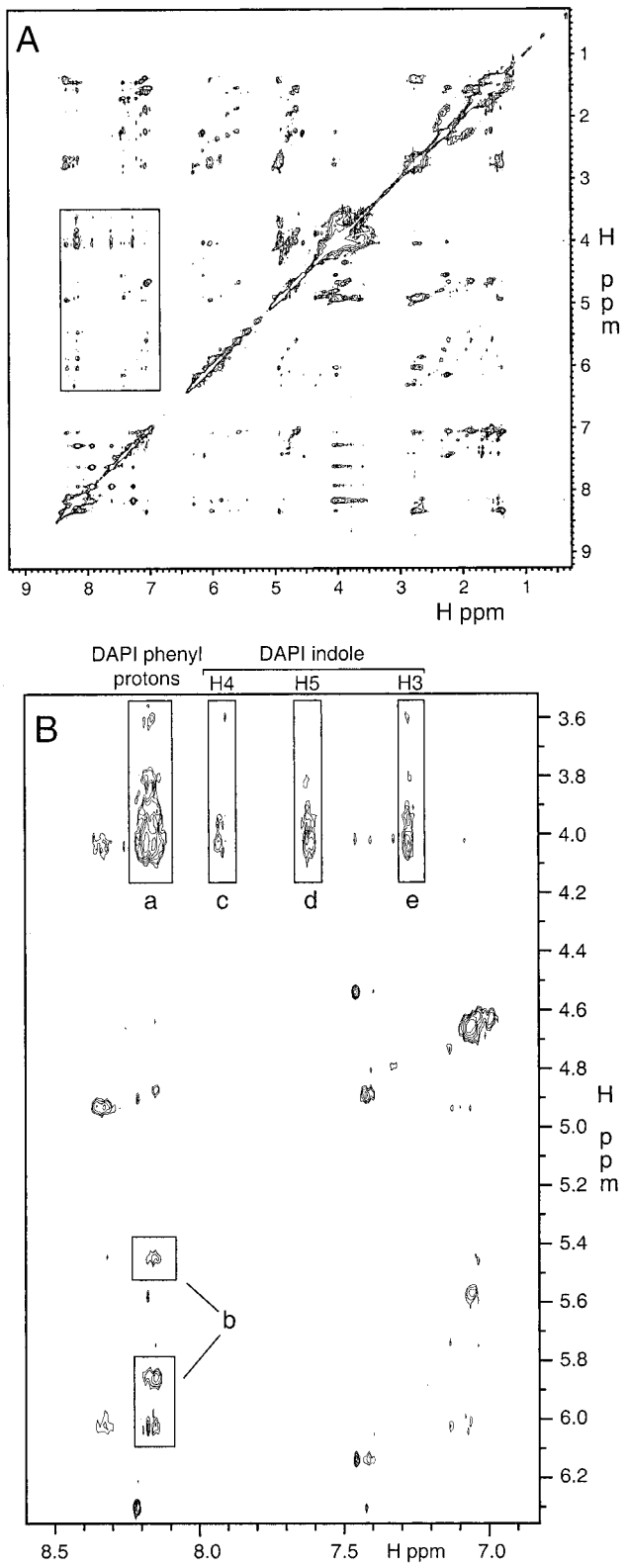

FIGURE 4: (A) NOESY spectrum of a 2:1 DAPI−$(ATT)_6$ complex acquired with a mixing time of 250 ms, in D_2O buffer, at 25 °C. (B) Expanded region indicated in spectrum A. Intermolecular drug−DNA NOEs are marked: (a) DAPI (phenyl protons)−DNA (H4′/H5′/H5″), (b) DAPI (phenyl protons)−DNA (H1′), (c) DAPI (H4)−DNA (H4′/H5′/H5″), (d) DAPI (H5)−DNA (H4′/H5′/H5″), and (e) DAPI (H3)−DNA (H4′/H5′/H5″).

The spectra of the complexes acquired at high temperatures also exhibit narrow resonances that can be attributed to DAPI imino (11.2 ppm) and amino (9 ppm) protons (*19*, *20*, *28*, *29*), providing evidence of their reduced rate of exchange with water protons upon binding to $(AAT)_6$.

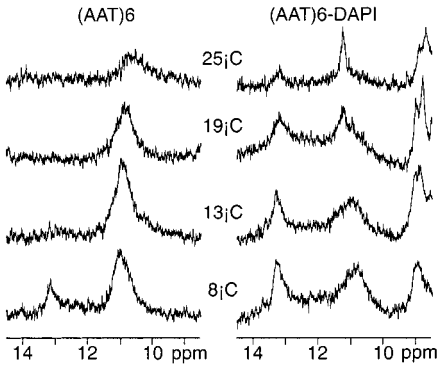

FIGURE 5: Imino proton spectra of $(AAT)_6$ and the 2:1 DAPI−$(AAT)_6$ complex. Spectra were acquired at different temperatures, with a 1−1 spin-echo pulse sequence to suppress the water signal.

Nonexchangeable proton resonances of $(AAT)_6$ are broadened but slightly shifted upon drug binding. In contrast, DAPI resonances are significantly upfield shifted in the complex (0.1−0.3 ppm).

UV Spectroscopy and Thermal Melting Studies. Figure 6 shows the melting curves of $(AAT)_6$, $(ATT)_6$, and $(AAT)_6$·$(ATT)_6$ in the absence and presence of DAPI, obtained by measuring the hyperchromic effect at 260 nm by increasing the temperature. A complete sigmoidal melting profile, indicative of a cooperative transition from a helix to coil state, is only observed for $(AAT)_6$·$(ATT)_6$ samples and the $(ATT)_6$−DAPI complex. In particular, the binding of DAPI shifts the sigmoidal melting profile of $(AAT)_6$·$(ATT)_6$ to higher temperatures, by increasing the T_m from 34 to 63 °C, but does not change significantly the hyperchromic effect induced by rising the temperature from 2 to 70 °C (about 39%) (Figure 6C). In contrast, the hyperchromic change of $(ATT)_6$ by increasing the temperature from 2 to 66 °C (23%) is strongly enhanced in the complex with DAPI (33%). In addition, the melting profile of $(ATT)_6$ assumes in the complex a typical sigmoidal shape of a base-paired to random coil transition (Figure 6B). At 37 °C, DAPI-free $(ATT)_6$ is almost all in a random coil conformation, whereas in the complex, $(ATT)_6$ is prevalently base-paired (T_m = 42 °C). The same effect on thermal stability of $(ATT)_6$ was also observed by the other minor groove binder Hoechst 33258 (T_m = 43 °C) (data not shown), suggesting that base-pairing induction of $(ATT)_6$ could be a general feature of classical minor groove binders. The relatively weak hyperchromic effect observed for free $(AAT)_6$ (16%) is increased by the addition of the drug to the oligomer solution (26%), but different from that of its complementary strand $(ATT)_6$, the melting profile in the presence of DAPI exhibits only the upper region of a sigmoidal shape (Figure 6A).

The DAPI absorption peak around 350 nm is red shifted and reduced in intensity upon binding to $(AAT)_6$, $(ATT)_6$, and $(AAT)_6$·$(ATT)_6$. A hypochromic effect of about 40% and a red shift of 20−30 nm of this signal have been reported for binding of DAPI to poly[d(GC)]$_2$ (*23*−*25*), while a hypochromic effect of about 12% and a red shift of about 12 nm for binding to poly[d(AT)]$_2$ are reported (*43*). The DAPI hypochromic effect observed in our experiments was higher for $(AAT)_6$ (17%) than for $(ATT)_6$ (11%) and $(AAT)_6$·$(ATT)_6$ (11%) samples, whereas the DAPI violet shift was

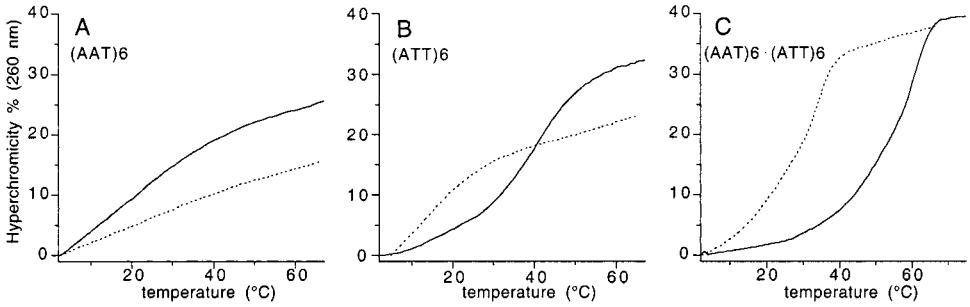

FIGURE 6: Melting curves of $(AAT)_6$, $(ATT)_6$, and $(AAT)_6$·$(ATT)_6$: (A) $(AAT)_6$ (dotted line) and the DAPI−$(AAT)_6$ complex (solid line), (B) $(ATT)_6$ (dotted line) and the DAPI−$(ATT)_6$ complex (solid line), and (C) $(AAT)_6$·$(ATT)_6$ (dotted line) and the DAPI−$(AAT)_6$·$(ATT)_6$ complex. The base pair:drug molar ratio of the complexes was 3.

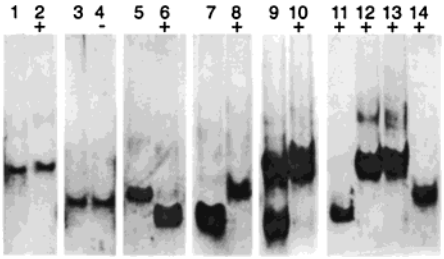

FIGURE 7: Nondenaturing polyacrylamide gel electrophoretic analysis. Electrophoretic mobility of $(AAT)_6$·$(ATT)_6$ (lane 1), $(AAT)_6$·$(ATT)_6$−DAPI (lane 2), $(AAT)_6$ (lane 3), $(AAT)_6$−DAPI (lane 4), $(ATT)_6$ (lane 5), $(ATT)_6$−DAPI (lane 6), $(AT)_5$ (lane 7), $(AT)_5$−DAPI (lane 8), $(AT)_9$ (lane 9), $(AT)_9$−DAPI (lane 10), $(ATT)_6$−DAPI (lane 11), $(AAT)_6$·$(ATT)_6$−DAPI (lane 12), $(AT)_9$−DAPI (lane 13), and $(AT)_5$−DAPI (lane 14). The gel was stained with silver. Lanes with DAPI−DNA samples with and without fluorescent bands are indicated by (+) and (−), respectively.

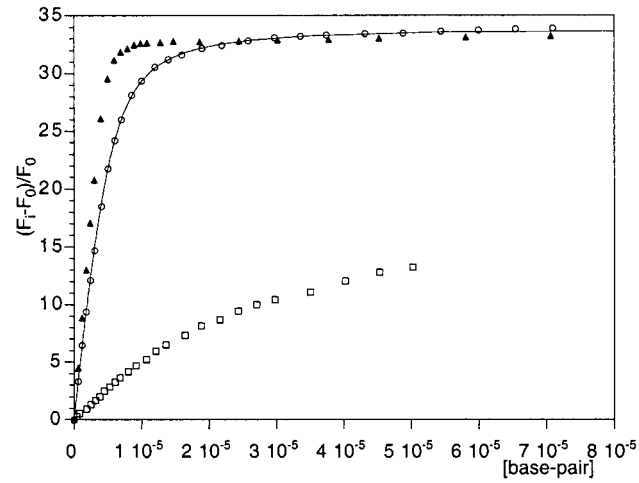

FIGURE 8: Reverse fluorescence titrations of DAPI (1 μM) with $(AAT)_6$·$(ATT)_6$ (▲), $(AAT)_6$ (□), and $(ATT)_6$ (○). $(F_i - F_0)/F_0$ is plotted vs base pair concentration (F_i is the observed fluorescence and F_0 the initial fluorescence of DNA-free DAPI). The curve represents the best two-parameter fit of $(ATT)_6$ experimental data with the theoretical model of Epstein (*39*).

higher for $(AAT)_6$·$(ATT)_6$ (16 nm) than for $(ATT)_6$ (12 nm) and $(AAT)_6$ (12 nm) samples.

Electrophoretic Mobility Studies. Figure 7 shows the relative electrophoretic mobilities of $(ATT)_6$, $(AAT)_6$, $(AAT)_6$·$(ATT)_6$, $(AT)_9$, and $(AT)_5$ as well as their complexes with DAPI in a silver-stained nondenaturing polyacrylamide gel. In the figure, the lanes containing fluorescent DAPI complexes, detected under UV light before silver staining, are indicated with (+) and the lanes of DAPI−DNA samples with no fluorescent bands are indicated with (−). As observed, a single fluorescent complex is detected in all the lanes containing DAPI (lanes 2, 6, 8, and 10−14) with the exclusion of the $(AAT)_6$−DAPI sample (lane 4) which does not exhibit visible fluorescent bands. The fluorescent $(ATT)_6$−DAPI complex (lane 11) migrates faster than the fluorescent $(AT)_5$−DAPI complex (lane 14). The $(AT)_9$−DAPI (lane 13) and $(AAT)_6$·$(ATT)_6$−DAPI (lane 12) fluorescent complexes exhibit similar electrophoretic mobilities and migrate more slowly than $(ATT)_6$−DAPI (lane 11) and $(AT)_5$−DAPI (lane 14) complexes. In the absence of DAPI, $(AAT)_6$ (lane 3) and $(ATT)_6$ (lane 5) migrate faster than $(AAT)_6$·$(ATT)_6$ (lane 1) but slower than $(AT)_5$ (lane 7). Different from the other oligomers, DAPI-free $(AT)_9$ shows two different electrophoretic species (lane 9): a slow-migrating species with the same mobility as $(AAT)_6$·$(ATT)_6$ (lane 1) and a fast-migrating species slightly faster than $(AT)_5$ (lane 7). The addition of DAPI to the DNA solutions determines changes in the electrophoretic mobility of all oligomers with the exclusion of $(AAT)_6$ which appear to be unaffected by the drug (lanes 3 and 4). In particular, the DAPI−$(ATT)_6$ complex (lane 6) migrates faster than DAPI-free $(ATT)_6$ (lane 5), whereas $(AAT)_6$·$(ATT)_6$ (lanes 1 and 2), $(AT)_5$ (lanes 7 and 8), and the slow-migrating species of $(AT)_9$ (lanes 9 and 10) exhibit a reduced mobility upon binding to DAPI. In the presence of ligand, $(AT)_9$ (lane 13) does not form the fast-migrating band. Finally, all the oligomers migrate at the expected speed in a denaturing gel of polyacrylamide (not shown).

Fluorescence and Binding Constants. Addition of $(ATT)_6$ and $(AAT)_6$·$(ATT)_6$ to a DAPI solution determines similar large increases in the intensity of the drug fluorescence signal (34- and 33-fold, respectively) (Figure 8) and the shifts of the maximum emission to lower wavelengths (about 20 nm) typical of DAPI binding to AT sequences (*44*). In contrast, binding of $(AAT)_6$ to DAPI causes a smaller increase in the drug fluorescence intensity (13-fold).

Figure 8 shows the fluorescence reverse titration of DAPI with $(ATT)_6$, $(AAT)_6$, and $(AAT)_6$·$(ATT)_6$ at a ligand concentration of 1 μM. The binding of $(AAT)_6$·$(ATT)_6$ to DAPI is nearly stoichiometric at the experimental condition so that four ligand sites per heteroduplex (4.6 bp per DAPI) were determined with good approximation. This is consistent with the stoichiometry of binding determined by NMR titration of $(ATT)_6$ with DAPI (see above) and with the binding site size of 4 bp previously reported for minor groove binding of DAPI to A·T sequences (*21*, *45*, *46*). The apparent binding constants estimated by the expression of Kelly et

al. (*38*), by considering two binding sites for 9 bp, were 3.4 $\times$ 10^6 and 2.9 $\times$ 10^7 M^{-1} for $(ATT)_6$ and $(AAT)_6$·$(ATT)_6$, respectively.

The $(ATT)_6$ experimental data were also fitted by the theoretical model of Epstein (*39*) by considering a site size of 4 bp and a lattice length of 9 bp. The best two-parameter fit of the experimental data, shown by a solid line in Figure 8, gives a binding constant value of 2 $\times$ 10^6 M^{-1} and a cooperativity parameter of 1.8, consistent with the estimated value obtained by using the expression of Kelly et al.

The weak increase in the intensity of the fluorescence signal of DAPI in titration experiments with $(AAT)_6$ reaches a plateau at a very high ligand:DNA molar ratio (Figure 8), and binding parameters were not determined.

DISCUSSION

DNA Base Pairing. NMR and UV-melting results indicate that both $(AAT)_6$ and $(ATT)_6$ oligomers adopt prevalently single-stranded non-hydrogen-bonded structures in the absence of the complementary strand and DAPI. As revealed by ^{1}H NMR imino proton spectra, a little component of hydrogen-bonded A·T base pairs is only found for $(AAT)_6$ at low temperatures (<11 °C) (Figure 5). Addition of DAPI to $(ATT)_6$ and $(AAT)_6$ solutions causes quite different results, showing an asymmetric effect of the ligand on the two strands of this class of triplet repeats. In the case of $(ATT)_6$, DAPI induces stable hydrogen-bonded base pairing. The appearance of DNA imino resonances at about 14 and 10.3 ppm, upon addition of DAPI to the $(ATT)_6$ solution (Figure 2), provides evidence of the formation of A·T Watson−Crick and T·T mismatch hydrogen-bonded base pairing, consistent with the NMR results previously reported for the minor groove complex of DAPI bound to the ATT·ATT site of $[d(GCGATTCGC)]_2$ (*20*). This is also supported by the observation of strong NOE contacts between the thymine imino proton of the A·T base pair and the adenine NH_2 (Figure 3).

Thermal melting studies also provide evidence of stable base pairing of $(ATT)_6$ in the DAPI complex. The strong and cooperative hyperchromic effect (33%) observed by increasing the temperature is indicative of a large degree of base unstacking and typical of hydrogen-bonded structures upon melting (Figure 6). In this regard, it should be noted that the T_m of $(ATT)_6$ in the complex (42 °C), under the experimental condition, is higher than that of the DAPI-free $(AAT)_6$·$(ATT)_6$ heteroduplex (37 °C). On the other hand, when the temperature is raised from 3 to 69 °C, DAPI-free $(ATT)_6$ exhibits a lower hyperchromic effect (23%) than in the complex (33%), indicating base stacking induced by DAPI. In addition, the large increase in the fluorescence quantum yield of DAPI upon binding to $(ATT)_6$ is characteristic of minor groove complexes and therefore indicative of base-paired structures. Therefore, from the results discussed above, we conclude that binding of DAPI to $(ATT)_6$ induces the conformational transition of the oligomer from single-stranded coil to monomeric or polymeric base-paired structures.

DAPI also favors hydrogen-bonded base pairing of $(AAT)_6$. In this case, the addition of DAPI causes an increase in the intensity of the ^{1}H NMR imino signal due to hydrogen-bonded A·T base pairs, but different from $(ATT)_6$−DAPI complexes, at 298 K it almost disappeared also at high drug:oligonucleotide molar ratios (Figure 5). This difference in the NMR thermal stability between $(ATT)_6$−DAPI and $(AAT)_6$−DAPI complexes is confirmed by UV melting studies. In the $(AAT)_6$−DAPI complex, the cooperative character of the melting profile is scarcely pronounced showing only the upper region of a sigmoidal shape. Moreover, UV melting experiments evidence a lower hyperchromic effect of the $(AAT)_6$ complex (25%) than of the $(ATT)_6$ (33%) and $(AAT)_6$·$(ATT)_6$ (39%) complexes. This is indicative of a lower degree of base stacking of $(AAT)_6$ than of $(ATT)_6$ and $(AAT)_6$·$(ATT)_6$ complexes at low temperatures.

Binding Geometry. As reported in the literature, DAPI binds DNA in at least two different ways which are well distinguished from each other by NMR and optical spectroscopy. DAPI binds preferentially DNA sites containing two or more consecutive A·T base pairs or T·T mismatches flanked by A·T base pairs by a minor groove binding geometry well characterized by X-ray and NMR spectroscopy (*19*, *20*, *26*−*28*). Different binding mechanisms have been proposed for the weaker interaction of DAPI with G·C or nonconsecutive A·T sequences: intercalation, major groove binding, and $\pi-\pi$ stacking interactions with double-helix ends (*21*−*25*).

Binding of DAPI to $(ATT)_6$ shows all the characteristic NMR results previously reported for binding of the drug into the minor groove of consecutive A·T base pairs (*19*, *20*, *28*). (a) Resonances of DNA protons lying in the minor groove (H1′ and H4′/H5′/H5″) are upfield shifted as a result of the ring current shielding effects of DAPI aromatic groups. (b) DAPI resonances are slightly shifted with respect to those of the free form and do not exhibit the strong upfield shifts typical of G·C-type binding (*23*, *29*). (c) Intermolecular DAPI−DNA NOEs involve only DNA protons H1′ and H4′/H5′/H5″ exposed in the minor groove. In addition, consistent with previously characterized minor groove complexes, H3, H4, and H5 DAPI indole protons exhibit intermolecular NOEs with only H4′/H5′/H5″ (Figure 4B), whereas phenyl protons exhibit NOEs with both H1′ and H4′/H5′/H5″ DNA protons. Since H1′ DNA protons lie deeper in the minor groove than H4′/H5′/H5″, this result agrees with the previously reported molecular structures of minor groove complexes in which DAPI lies in the minor groove with its major axis nearly isohelical and the NH indole proton oriented toward the DNA helix axis and H3, H4, and H5 protons toward the external of the groove next to H4′/H5′/H5″ DNA protons (*19*, *20*, *26*−*28*). Optical spectroscopy results are also consistent with a minor groove binding of DAPI to $(ATT)_6$. The large increase in the fluorescence quantum yield (34-fold) and the narrowing of the shape of the emission spectrum observed when DAPI binds $(ATT)_6$ are typical of AT minor groove complexes (*44*). Moreover, melting of the double helix is accompanied by the blue shift (20 nm) and the increase in the intensity (20%) of the DAPI absorption peak around 350 nm, as expected for the dissociation of minor groove complexes.

The results for the $(AAT)_6$ strand do not appear to be simply interpretable as in the case of $(ATT)_6$. The addition of $(AAT)_6$ to a DAPI solution causes a small increase in the drug fluorescence intensity at 15 °C, indicating a weak minor groove binding constant and/or different binding mecha-

nisms. However, this relatively small enhancement of DAPI fluorescence upon binding to $(AAT)_6$ is accompanied by a strong hypochromicity of the drug absorption signal at 350 nm (17%), larger than those of strongly fluorescent $(ATT)_6$ (11%) and $(AAT)_6$·$(ATT)_6$ (11%) complexes. This suggests the presence of binding mechanisms other than minor groove interaction. It has been proposed that the large increase in DAPI fluorescence by minor groove binding to DNA should be due to the shielding of the drug from solvent molecules (*47*). This could suggest a higher accessibility of DAPI to water molecules when it is bound to $(AAT)_6$ than when it is bound to $(ATT)_6$ and $(AAT)_6$·$(ATT)_6$. On the other hand, small or no fluorescence enhancement, associated with higher hypochromicity of the DAPI signal at 350 nm with respect to AT sequences, has been reported for binding of DAPI to poly[d(GC)]$_2$, poly(rA)·poly(rU), and poly(rA) and attributed to a binding mechanism other than minor groove interaction (*23*, *25*, *44*, *48*, *49*). NMR results also provide evidence of different binding geometries between $(AAT)_6$− and $(ATT)_6$− DAPI complexes. Different from $(ATT)_6$ and minor groove DAPI complexes previously studied, at 298 K NMR proton resonances of the drug in the $(AAT)_6$ complex appear upfield shifted with respect to the free form (at 286 K they are too broad and were not assigned). However, the magnitude of the DAPI resonance shifts at 298 K (0.1−0.3 ppm) is not comparable with those previously observed with GC-rich sequences (0.4−0.9 ppm) and attributed to an intercalation binding mechanism (*21*, *29*), while the magnitude is quite similar to that observed when DAPI binds to single-stranded oligomer d(AAACCC) (0.2−0.35 ppm) (data not shown). On the other hand, nonexchangeable $(AAT)_6$ resonances at 298 K are strongly broadened upon addition of DAPI but only slightly shifted, suggesting the minor involvement of deoxyribose and base protons in the binding. Also, the weak imino signal observed at 281 K in the absence of DAPI and attributed to A·T base pairs is increased upon addition of DAPI but very slightly downfield shifted (Figure 5). This is in contrast to the strong upfield shifts of DNA imino signals expected for intercalation binding mechanisms (*23*, *29*, *50*) or downfield shifts induced by minor groove binding (*19*−*21*, *28*, *50*), but it is consistent with binding of DAPI to the outside of the DNA in an aspecific manner (*50*). Considering that exchangeable proton resonances of DAPI are well observed at 298 K, suggesting their involvement in intermolecular hydrogen bonds, we conclude that DAPI interacts with $(AAT)_6$ by a binding mechanism that favors weak base pairing but does not involve directly oligomer bases, consistent with external binding with the phosphodiester chain by electrostatic and hydrogen bond interactions.

Secondary Structure of Oligomers. The results discussed above provide evidence that DAPI induces base pairing of $(ATT)_6$ by a minor groove binding mechanism. Base pairing could be mainly expected from both monomeric hairpin and dimeric homoduplex structures. The results of electrophoretic analyses performed at 4 and 25 °C provide evidence that DAPI induces the formation of a stable monomeric hairpin structure of $(ATT)_6$. As expected for the hairpin structure, the $(ATT)_6$−DAPI complex exhibits about the same mobility as the $(AT)_5$−DAPI complex and migrates much faster than $(AAT)_6$·$(ATT)_6$ and $(AT)_9$ complexes (Figure 7). Although both random coil and monomeric hairpin structures should migrate faster than the dimeric homoduplex (*51*), random coil can be excluded since the $(ATT)_6$−DAPI complex migrates by maintaining its fluorescent property characteristic of minor groove complexes of base-paired structures. In addition, the higher electrophoretic mobility of the $(ATT)_6$ complex with respect to the DAPI-free $(ATT)_6$ (Figure 8) is consistent with the relative mobility of hairpin and coil forms reported for $(GGA)_n$ and $(GGGA)_n$ DNA sequences (*52*). On the other hand, the higher mobility of the DAPI−$(ATT)_6$ complex with respect to DAPI-free $(ATT)_6$ cannot be simply attributable to the DAPI interaction since DAPI complexes of $(AAT)_6$·$(ATT)_6$, $(AT)_5$, and $(AT)_9$ migrate slower than the respective DAPI-free duplex (Figure 8). The presence of a single electrophoretic species of the $(ATT)_6$−DAPI complex along with a monophasic single cooperative structural transition observed by UV melting experiments excludes the presence of dimeric homoduplex structures. Moreover, in agreement with a hairpin secondary structure, the imino signal assigned to unpaired thymines (11 ppm) does not disappear completely also at high DAPI:$(ATT)_6$ molar ratios.

Different from those of the other oligomers, the electrophoretic mobility of $(AAT)_6$ is not changed by the presence of DAPI, and no fluorescent species were observed. This suggests minor structural changes of $(AAT)_6$ induced by DAPI or very labile complexes also at 4 °C.

In contrast to the results for $(ATT)_6$, electrophoretic analysis of $(AT)_9$ samples shows that DAPI favors the dimeric homoduplex structure of AT dinucleotide repeats against the monomeric hairpin.

Finally, electrophoretic analysis of $(AAT)_6$·$(ATT)_6$− and $(AT)_9$−DAPI complexes (lanes 12 and 13) exhibits secondary slow-migrating weak bands which suggest the formation of minor multimeric DNA structures.

$(ATT)_6$ Conformation in the Complex. Weak or no intranucleotide H1′−H6/H8 and H2″−H4′ NOEs are consistent with a prevalent anti conformation of glycosidic torsion angles and C2′-endo furanose ring pucker, suggesting a local right-handed B-like conformation.

Molecular Modeling of the $(ATT)_6$−DAPI Complex. To provide a structural basis for $(ATT)_6$ hairpin−DAPI interaction, we submitted 12 potential complexes to molecular dynamics simulations as reported in Experimental Procedures. Figure 9 shows the lowest-energy complex of the 12 final structures of calculations. During all simulations, DAPI molecules maintain their deep insertion into the minor groove, although an isohelical shift of about 1 bp along the groove has been observed for one ligand in five final structures. With one exception, the DNA hairpin of final structures is characterized by a loop of two bases (central AT in the sequence) and a stem constituted by five well-stacked A·T Watson−Crick and three T·T wobble base pairs. The hairpin stem exhibits C1′−C1′ base pair distances that are shorter than canonical B-DNA (10.8 Å), especially at T·T mismatch sites (about 8.9 Å), in agreement with those previously reported for T·T mismatches of d(GCCACTAGCTC)·d(GAGCTTGTGGC) (9.4 Å) (*53*) and [d(GCGATTCGC)]$_2$ complexed with DAPI (8.9 Å) (*20*). All final structures are characterized by favorable intermolecular van der Waals energies (ranging from −84 to −71 kcal/mol) and 8−15 intermolecular hydrogen bonds, 4−8 of which involve O2 proton acceptors of thymines. From the results of molecular modeling, a ligand site size of 4 bp accounts well

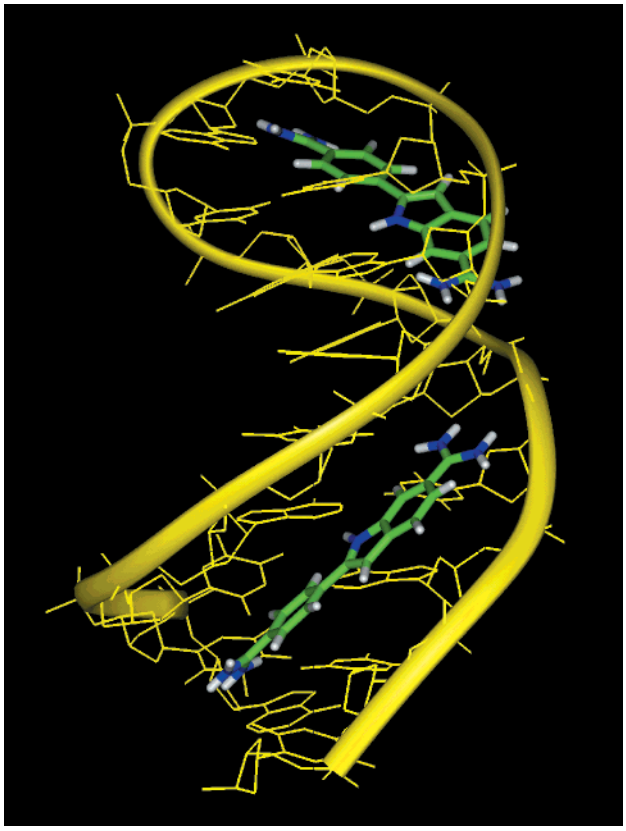

FIGURE 9: Lowest-energy final structure of 12 molecular dynamics simulations of DAPI−$(ATT)_6$ complexes.

for a low level of DAPI−DAPI intermolecular electrostatic repulsion.

Conclusions. Our results show that individual $(AAT)_6$ and $(ATT)_6$ strands do not exhibit the propensity to adopt stable secondary structures other than single-stranded random coil forms. These results appear to be dramatically changed when individual AAT and ATT strands interact with DAPI. $(ATT)_6$ adopts stable monomeric hairpin structure (T_m = 42 °C) favored by two DAPI molecules inserted into the minor groove with a strong binding affinity ($K_a = 3.4 \times 10^6$). The ability of DAPI to strongly bind and stabilize $(ATT)_6$ base-paired structures appears to be related to the favorable property of the minor groove of T·T mismatches and A·T base pairs: (a) its narrow and deep shape (*20*) which promotes favorable van der Waals contacts with ligands, (b) its negative electrostatic potential that favors interaction with cationic ligands, and (c) its elevated number of hydrogen bond acceptors that contributes to the binding affinity and base pair stability by involving simultaneously both strands in the formation of intermolecular hydrogen bonds (*20*). The results obtained with the complementary $(AAT)_6$ strand indicate that substitution of T·T with an A·A mismatch disfavors DAPI minor groove binding, leading to more labile complexes and less stable base pairing. Since A·A and T·T mismatches cause similar destabilizing effects on the double helix (*54*−*56*), this result should be mainly attributable to the more favorable properties of T·T than of the A·A minor groove in binding DAPI. C1′−C1′ distances of A·A mismatch are 3 Å larger than that of T·T mismatches and 1.5 Å larger than that of A·T Watson−Crick base pairs (*53*). This suggests that a significant contribution to the observed relatively low affinity of A·A-containing sequences could be attributable to the reduced level of favorable intermolecular van der Waals interactions between DAPI aromatic rings and the sides of its wide minor groove. The importance of this structural feature in affecting DAPI minor groove binding affinity has been previously suggested to explain the considerable less favorable binding property of the wide and shallow minor groove of poly(AU) with respect to poly(AT) (*44*). In addition, in all minor groove structures previously reported (*19*, *20*, *26*−*28*), thymine O2 is the DNA group most frequently involved in intermolecular hydrogen bonds with DAPI. This suggests that thymine O2 could play a non-negligible role in the stability of DAPI minor groove complexes and could be a more suitable hydrogen bond acceptor than adenine N3 in favoring binding and base pair stability.

Biological Implications. As reported in the literature, the major characteristic of GC-rich triplet repeats that undergo extensive expansion is the propensity, in vitro and in vivo, to form stable hairpins with a threshold energy which favors slippage during DNA replication processes and that are inefficiently repaired in comparison with looped unpaired structures (*57*). Although the AAT·ATT triplet repeat is not yet found to undergo to extensive expansion in vivo, as found for triplet repeats associated with human diseases, it has recently been reported that destabilizing factors of double-stranded DNA such as low salt concentration and high temperature have the properties to favor expansion of both strands belonging to AAT·ATT triplet repeats up to 1000-fold during DNA replication in vitro (*8*). In agreement with our results showing no secondary base-paired structures of individual $(ATT)_6$ and $(AAT)_6$ strands, the unstructured loop should be efficiently repaired in vivo, explaining the inconsistency found between expansion of AAT·ATT repeats in vitro and in vivo. On the other hand, the hairpin structure induced by DAPI on $(ATT)_6$ shows the same structural features reported for the hairpin of CTG repeats which undergo extensive expansion in vivo. Both are characterized by high thermal stability and the presence of stable well-stacked T·T mismatches flanked by Watson−Crick base pairs. The observation that long tracts of CTG·CAG repeats block the replication fork in *Escherichia coli* (*58*) and affect transcription processes (*59*) suggests that the propensity of $(ATT)_6$ to adopt similar stable secondary structures, modulated by DNA ligands, could have the potential to influence genetic processes. In this regard, it should be noted that the affinity of binding of DAPI to the $(ATT)_6$ strand is higher than that reported in the literature for poly[d(GC)]$_2$ ($K_a = 1.2 \times 10^5$ M^{-1}) (*44*), indicating that single-stranded regions of ATT repeats can be considered a more favorable DAPI genomic target than GC base pairs. This result may have biological implications considering that the AAT·ATT repeat is the only triplet repeat which shows a propensity to adopt non-hydrogen-bonded structures in plasmids (*10*). Such a distinctive in vivo instability of the AAT·ATT double helix could favor the exposure of ATT single-stranded tracts to DNA ligands with the potential to induce biologically active secondary structures. These new structural properties of the ATT triplet repeat should be considered in attempting to explain biological effects of minor groove binders as well as in clarifying the genetic role of microsatellite DNA in relation to its secondary structure.

ACKNOWLEDGMENT

We thank Dr. Daniela Orru' for helpful discussion, Fabio Bertocchi for technical assistance with the 400 MHz NMR instrument, and Dr. Lorenzo Stella for help in fluorescence studies. The MURST PRIN project "Structural Biology" and the Target Project of CNR "Biotechnology" are acknowledged.

REFERENCES

1. Strachan, T., and Read, A. P. (1996) *Human Molecular Genetics*, John Wiley and Sons, New York.
2. Sinden, R. R. (1999) *Am. J. Hum. Genet. 64*, 346−353.
3. Gacy, A. M., Goellner, G., Juranic, N., Macura, S., and McMurray, C. T. (1995) *Cell 81*, 533−540.
4. Moore, H., Greenwell, P. W., Liu, C.-P., Arnheim, N., and Petes, T. D. (1999) *Proc. Natl. Acad. Sci. U.S.A. 96*, 1504−1509.
5. Mitas, M. (1997) *Nucleic Acids Res. 25*, 2245−2253.
6. Pearson, C. E., and Sinden, R. R. (1998) *Curr. Opin. Struct. Biol. 8*, 321−330.
7. Gastier, J. M., Pulido, J. C., Sunden, S., Brody, T., Buetow, K. H., Murray, J. C., Weber, J. L., Hudson, T. J., Sheffield, V. C., and Duyk, G. M. (1995) *Hum. Mol. Genet. 4*, 1829−1836.
8. Lyons-Darden, T., and Topal, M. D. (1999) *Nucleic Acids Res. 27*, 2235−2240.
9. Lyons-Darden, T., and Topal, M. D. (1999) *J. Biol. Chem. 274*, 25975−25978.
10. Ohshima, K., Kang, S., Larson, J. E., and Wells, R. D. (1996) *J. Biol. Chem. 271*, 16784−16791.
11. Kapuscinski, J. (1995) *Biotech. Histochem. 70*, 220−233.
12. Parolin, C., Montecucco, A., Chiarocchi, G., Pedrali-Noy, G., Valisena, S., Palumbo, M., and Palù, G. (1990) *FEMS Microbiol. Lett. 68*, 341−346.
13. Straney, D. C., and Crothers, D. M. (1987) *Biochemistry 26*, 1987−1995.
14. Chiang, S.-Y., Welch, J., Rausher, F. J., and Beerman, T. A. (1994) *Biochemistry 33*, 7033−7040.
15. Storl, K., Storl, J., Zimmer, C. H., and Lown, J. W. (1993) *FEBS Lett. 317*, 157−162.
16. Woynarowski, J. M., McHugh, M., Sigmund, R. D., and Beerman, T. A. (1989) *Mol. Pharmacol. 35*, 177−182.
17. McHugh, M. M., Woynarowski, R. D., and Beerman, T. A. (1989) *Biochem. Pharmacol. 38*, 2323−2328.
18. Parolin, C., Zanotti, G., and Palù, G. (1995) *Biochem. Biophys. Res. Commun. 208*, 332−338.
19. Trotta, E., D'Ambrosio, E., Del Grosso, N., Ravagnan, G., Cirilli, M., and Paci, M. (1993) *J. Biol. Chem. 268*, 3944−3951.
20. Trotta, E., and Paci, M. (1998) *Nucleic Acids Res. 26*, 4706−4713.
21. Wilson, W. D., Tanious, F. A., Barton, H. J., Jones, R. L., Fox, K., Wydra, R. L., and Strekowski, L. (1990) *Biochemistry 29*, 8452−8461.
22. Wilson, W. D., Tanious, F. A., Barton, H. J., Wydra, R. L., Jones, R. L., Boykin, D. W., and Strekowski, L. (1990) *Anti-Cancer Drug Des. 5*, 31−42.
23. Wilson, W. D., Tanious, F. A., Barton, H. J., Strekowski, L., and Boykin, D. W. (1989) *J. Am. Chem. Soc. 111*, 5008−5010.
24. Jansen, K., Nordén, B., and Kubista, M. (1993) *J. Am. Chem. Soc. 115*, 10527−10530.
25. Kim, S. K., Eriksson, S., Kubista, M., and Nordén, B. (1993) *J. Am. Chem. Soc. 115*, 3441−3447.
26. Larsen, T. A., Goodsell, D. S., Cascio, D., Grzeskowiak, K., and Dickerson, R. E. (1989) *J. Biomol. Struct. Dyn. 7*, 477−491.
27. Vlieghe, D., Sponer, J., and Van Meervelt, L. (1999) *Biochemistry 38*, 16443−16451.
28. Trotta, E., D'Ambrosio, E., Ravagnan, G., and Paci, M. (1996) *J. Biol. Chem. 271*, 27608−27614.
29. Trotta, E., D'Ambrosio, E., Ravagnan, G., and Paci, M. (1995) *Nucleic Acids Res. 23*, 1333−1340.
30. Kastrup, R. V., Young, M. A., and Krugh, T. R. (1978) *Biochemistry 17*, 4855−4865.
31. Latt, S. A., and Wohlleb, J. C. (1975) *Chromosoma 52*, 297−316.
32. Marion, D., and Wutrich, K. (1983) *Biochem. Biophys. Res. Commun. 113*, 967−974.
33. Bax, A., and Davis, D. G. (1986) *J. Magn. Reson. 65*, 355−360.
34. Braunschweiler, L., and Ernst, R. R. (1983) *J. Magn. Reson. 53*, 521−528.
35. Jeener, J., Meier, B. H., Bachmann, P., and Ernst, R. R. (1979) *J. Chem. Phys. 71*, 4546−4553.
36. Sklenar, V., and Bax, A. (1987) *J. Magn. Reson. 74*, 469−479.
37. Delaglio, F., Grzesiek, S., Vuister, G. W., Zhu, G., Pfeifer, J., and Bax, A. (1995) *J. Biomol. NMR 6*, 277−293.
38. Kelly, R. C., Jensen, D. E., and von Hippel, P. H. (1976) *J. Biol. Chem. 251*, 7240−7250.
39. Epstein, I. R. (1978) *Biophys. Chem. 8*, 327−339.
40. Mohan, S., and Yathindra, N. (1994) *J. Biomol. Struct. Dyn. 11*, 849−867.
41. Cornelis, A. G., Haasnoot, J. H. J., den Hartog, J. F., de Rooij, M., van Boom, J. H., and Cornelis, A. (1979) *Nature 281*, 235−236.
42. Roberts, G. C. K. (1993) *NMR of Macromolecules-A pratical Approach*, pp 217−288, IRL Press, Oxford, U.K.
43. Eriksson, S., Kim, S. K., Kubista, M., and Nordén, B. (1993) *Biochemistry 32*, 2987−2998.
44. Tanious, F. A., Veal, J. M., Buczak, H., Ratmeyer, L. S., and Wilson, W. D. (1992) *Biochemistry 31*, 3103−3122.
45. Portugal, J., and Waring, M. J. (1988) *Biochim. Biophys. Acta 949*, 158−168.
46. Jeppesen, C., and Nielsen, P. E. (1989) *Eur. J. Biochem. 182*, 437−444.
47. Barcellona, M. L., and Gratton, E. (1990) *Eur. Biophys. J. 17*, 315−323.
48. Sehlstedt, U., Kim, S. K., and Nordén, B. (1993) *J. Am. Chem. Soc. 115*, 12258−12263.
49. Kapuscinski, J. (1990) *J. Histochem. Cytochem. 38*, 1323−1329.
50. Feigon, J., Denny, W. A., Leupin, W., and Kearns, D. R. (1984) *J. Med. Chem. 27*, 450−465.
51. Maniatis, T., Jeffrey, A., and van de Sande, H. (1975) *Biochemistry 14*, 3787−3794.
52. Huertas, D., and Azorin, F. (1996) *Biochemistry 35*, 13125−13135.
53. Gervais, V., Cognet, J. A. H., Le Bret, M., Sowers, L. C., and Fazakerley, G. V. (1995) *Eur. J. Biochem. 228*, 279−290.
54. Aboul-ela, F., Koh, D., and Tinoco, I. (1985) *Nucleic Acids Res. 13*, 4811−4824.
55. Werntges, H., Steger, G., Riesner, D., and Fritz, H.-J. (1986) *Nucleic Acids Res. 14*, 3773−3790.
56. Ikuta, S., Takagi, K., Wallace, R. B., and Itakura, K. (1987) *Nucleic Acids Res. 15*, 797−811.
57. McMurray, C. T. (1999) *Proc. Natl. Acad. Sci. U.S.A. 96*, 1823−1825.
58. Samadashwily, G. M., Raca, G., and Mirkin, S. M. (1997) *Nat. Genet. 17*, 298−304.
59. Parsons, M. A., Sinden, R. R., and Izban, M. G. (1998) *J. Biol. Chem. 273*, 26998−27008.

BI0001473